Swashplate Actuator Failure Compensation for UH-60 Black Hawk in Cruise using Horizontal Stabilator

Praneet Vayalali PhD Student
Michael McKay PhD Student
Jayanth Krishnamurthi PhD Candidate
Farhan Gandhi Redfern Chair in Aerospace Engineering

Center for Mobility with Vertical Lift (MOVE)
Rensselaer Polytechnic Institute
Troy, NY United States

ABSTRACT

A flight simulation model for the UH-60 Black Hawk based on Sikorsky's GenHel model is modified to simulate a locked failure of a main rotor swashplate servo actuator and is compensated by using the stabilator as a redundant control effector. Steady state trim analysis is performed to demonstrate feasibility of trimmed flight in various conditions with different locked servo actuator positions for the forward, aft, and lateral actuators. A model-following, linear dynamic inversion controller is implemented and modified to account for locked actuator position. Post-failure, the control mixing and feed-forward control coupling terms are reconfigured to partially reallocate the control authority in the longitudinal axis from the main rotor longitudinal cyclic to a symmetric deflection of the stabilator. This is done by manipulation of only the control allocation relating pilot stick inputs to servo actuator positions, the feedback control gains and mechanical rigging between servo actuators and rotor pitch controls remain identical to the baseline controller. Flight simulation results demonstrate the ability of this reconfiguration to compensate for locked failure of the forward main rotor swashplate servo actuator, as well as the ability of the aircraft to decelerate from cruise at 120 knots to 50 knots which is less than the published safe rolling landing speed of 60 knots. A similar range of locked positions of the forward and aft actuators is demonstrated to be feasible for aircraft recovery using control of the stabilator. Feasibility of aircraft recovery for locked positions of the lateral servo actuator is also considered.

NOTATION

$\vec{x}$	State Vector
$\vec{u}$	Control Stick Input Vector
δ_{lat}	Lateral Stick
δ_{lon}	Longitudinal Stick
δ_0	Collective Stick
δ_{ped}	Pedal Stick
$\delta_{throttle}$	Throttle
θ_0	Collective Pitch
θ_{1c}	Lateral Cyclic Pitch
θ_{1s}	Longitudinal Cyclic Pitch
θ_{ped}	Tail Rotor Collective Pitch
θ_{slew}	Stabilator Slew Schedule Pitch Incidence
s_{lat}	Lateral Actuator Position
s_{fwd}	Forward Actuator Position
s_{aft}	Aft Actuator Position
s_{ped}	Pedal Actuator Position
s_{fail}	Failed Actuator Position
$M_{\theta/S}$	Mechanical Mixer
$M_{S/u}$	Control Mixer

Presented at the AHS International 74th Annual Forum & Technology Display, Phoenix, Arizona, USA, May 14–17, 2018.

INTRODUCTION

Improving survivability under conditions such as control failure or control surface damage has been a well-researched topic for fixed wing aircraft over the past few decades. From 1984-1993, the United States Air Force conducted a series of tests under the *Self-Repairing Flight Control System Program* (SRFCS) to design and test a reconfigurable control mixer using a modified pseudo-inverse that adds constraints to prevent control saturation and minimize cross-coupling, using the available control power. This allows fixed-wing aircraft with enough surplus control surfaces and available power to maintain trimmed flight despite failure or loss of a control surface (Refs. 1, 2). Similar research has been conducted since then (Ref. 3), including the Reconfigurable Control for Tailless Fighter Aircraft (RESTORE) which used the experimental X-36 aircraft as a test-bed (Ref. 4). RESTORE demonstrated the capabilities of a neural network to reconfigure the control laws after simulated actuator failures had locked a control effector in place.

While reconfiguration after control failure is a thoroughly explored subject for fixed-wing aircraft, very limited research has been conducted in parallel for application to rotary-wing aircraft. Hess (Ref. 5) attributes this lack of parallel work to the lack of redundant control effectors on conventional helicopters. The study focused on developing a pseudo-sliding mode control system for a UH-60A helicopter in hover that

was shown to be robust in the presence of significant variation in actuators, control system, vehicle characteristics, and sensors, demonstrating a degradation in the handling qualities. Heiges' study (Ref. 6) explores the possibility of reconfiguration in hover for rotors with two servo-flaps on each blade. Assuming zero change in the state sensitivity matrix (A) in the event of failure, the study demonstrated that fault detection and reconfiguration strategies developed for fixed-wing aircraft, such as using peudo-inverse control allocation to regain performance (does not guarantee stability), can be applied if requisite redundancies exist. Enns and Si (Ref. 7) describe a swashplate reconfiguration strategy (changing control mixer) that controls any two of the three main rotor control axes for any main rotor actuator failure. The study focuses on a particular swashplate reconfiguration solution where attitude control (pitch and roll) is retained, whereas vertical control is sacrificed. Vertical control is then achieved by one of two methods: flight to a longitudinal velocity that supports the desired vertical velocity or the use of rotor speed to change the main rotor's thrust to perform limited closed-loop vertical control. The study demonstrates reconfiguration after failure with a PID and a neural network based controller.

Reconfiguration in advanced high-speed compound rotorcraft configurations can be accomplished through use of the ailerons, stabilator pitch, and propellers to trim rotor produced forces and moments (Ref. 8). Drozeski et al. (Ref. 9) focuses on using neural networks to detect a finite number of predetermined faults (fault detection and isolation), and applies appropriate restructuring and reconfiguration through a fault tolerant adaptive controller to stabilize an unmanned rotary-wing aerial vehicle. Qi et al. (Ref. 10) give a comprehensive review on fault diagnosis and fault tolerant control methods for manned and unmanned helicopters discussing techniques like adaptive control, predictive control, and model matching fault tolerant controls.

The current study seeks to examine whether control actuator failure on a rotary-wing aircraft with some degree of redundancy can be compensated by reallocation of the control mixing alone, without any reconfiguration in feedback control laws (control gains), whatsoever. The specific example considered is that of a UH-60 Black Hawk helicopter in cruise. With its large horizontal stabilator able to input pitching moments on the aircraft (as well as augment lift), following appropriate modeling developments, the ability of the stabilator to compensate for failure in swashplate longitudinal control is analyzed and assessed through flight simulation. Use of differential stabilator concept to compensate for failure in swashplate lateral control is also explored.

APPROACH

Modeling

A UH-60A Black Hawk simulation model developed by Krishnamurthi and Gandhi (Ref. 11), which is a derivative of Sikorsky's GenHel model (Ref. 12), is used in this study. The model includes a non-linear, blade element representation of a single main rotor with articulated blades using airfoil table lookup. The blades themselves are approximated to be rigid, undergoing rotations about offset hinges. The 3-state Pitt-Peters dynamic inflow model (Ref. 13) is used to represent the induced velocity distribution on the rotor disk. The tail rotor thrust and torque are based on the closed-form Bailey rotor (Ref. 14) with a Pitt-Peters 1-state dynamic inflow model. The rigid fuselage and empennage (horizontal and vertical tail) forces and moments are implemented as look-up tables based on wind tunnel data from the GenHel model (Ref. 12). A simple 3-state turbine engine model given by Padfield (Ref. 15) is used for the propulsion dynamics, with the governing time constants approximated based on the GenHel engine model. The governing equations of motion are given by

$$\begin{aligned} \dot{\vec{x}} &= f(\vec{x},\vec{u}) \\ \vec{y} &= g(\vec{x},\vec{u}) \end{aligned} \tag{1}$$

where $\vec{y}$ is a generic output vector. The state vector $\vec{x}$, is given by

$$\begin{aligned} \vec{x} = [&u,v,w,p,q,r,\phi,\theta,\psi,X,Y,Z,\beta_0,\beta_{1s},\beta_{1c},\beta_d,\dot{\beta}_0,\dot{\beta}_{1s}, \\ &\dot{\beta}_{1c},\dot{\beta}_d,\lambda_0,\lambda_{1s},\lambda_{1c},\lambda_{0_{TR}},\Omega,\chi_f,Q_e]^T \end{aligned} \tag{2}$$

The state vector comprises of :

- 12 fuselage states $(u,v,w,p,q,r,\phi,\theta,\psi,x,y,z)$,
- 11 rotor states $(\beta_0,\beta_{1s},\beta_{1c},\beta_d,\dot{\beta}_0,\dot{\beta}_{1s},\dot{\beta}_{1c},\dot{\beta}_d,\lambda_0,\lambda_{1s},\lambda_{1c})$,
- 1 tail rotor inflow state $(\lambda_{0_{TR}})$, and
- 3 engine states (Ω,χ_f,Q_e).

The control stick input vector is given by

$$\vec{u} = [\delta_{lat},\delta_{lon},\delta_{col},\delta_{ped},\delta_{throttle}]^T \tag{3}$$

Validation of the baseline simulation model was performed in Ref. 11 against a trim sweep of flight test and GenHel data from Ref. 16, for a gross weight of 16,000 lbs and altitude of 5,250 ft.

Actuator geometry

Collective, lateral and longitudinal blade pitch $(\theta_0,\theta_{1c},\theta_{1s})$ are achieved by moving the base of the pitch link from the reference plane of the level swashplate. The non-rotating swashplate orientation is fully defined by the height of the swashplate where three mechanical linkages, also known as servo actuators, $(s_{lat},s_{fwd},s_{aft})$ actuate to transmit pilot control, as shown in Fig. 1. The servo actuators are related to the blade pitch controls $(\theta_0,\theta_{1c},\theta_{1s})$ by Eqs. 4-9. These equations demonstrate that the independent control of θ_0, θ_{1c}, and θ_{1s} is attainable with full control of s_{lat}, s_{fwd}, and s_{aft}.

$$\theta_{1c} \propto \frac{(s_{fwd}+s_{aft})}{2} - s_{lat} \quad (4) \qquad s_{lat} \propto \theta_0 - \theta_{1c} \quad (7)$$

$$\theta_{1s} \propto \frac{(s_{fwd}-s_{aft})}{2} \quad (5) \qquad s_{fwd} \propto \theta_0 + \theta_{1s} \quad (8)$$

$$\theta_0 \propto \frac{(s_{fwd}+s_{aft})}{2} \quad (6) \qquad s_{aft} \propto \theta_0 - \theta_{1s} \quad (9)$$

To produce an increase in collective pitch (θ_0) without changing the cyclic pitches, all three actuators need to be raised the same amount. Isolated increases in longitudinal cyclic pitch (θ_{1s}) result from a differential between the forward and aft actuators, while isolated lateral cyclic pitch (θ_{1c}) variation is accomplished by changing the lateral actuator position.

The servo naming convention is given relative to the primary effect that each actuator has on the flapping of the rotor (Fig. 1). Increases in the forward actuator height will increase longitudinal cyclic pitch and the rotor will flap up in the front of the disk, increases in the lateral actuator height will increase lateral cyclic pitch and lateral blade flapping, and increases in the aft actuator height will reduce longitudinal cyclic pitch and produce a higher flapping angle in the rear.

Servo actuator failure

The type of actuator failure addressed in the present study is referred to as a *locked condition*, where the input signal to a control actuator yields no response, as the actuator position is locked in place. This type of actuator failure results in a loss of independent control of the three blade pitches ($\theta_0, \theta_{1c}, \theta_{1s}$) as seen in Eqs. 4-9. Independent control of one is possible (over a certain range), but the two remaining blade pitches are governed by a constraint equation. For example, in the case of s_{fwd} or s_{aft} locked in place, lateral cyclic pitch (θ_{1c}) remains independently controllable (by use of s_{lat}), while longitudinal cyclic (θ_{1s}) and collective pitch (θ_0) become coupled. When the actuator is locked mid-flight, the control mixer can be reconfigured such that the stick input corresponding to the affected axis is remapped to a redundant control effector, *without any reconfiguration in the feedback control law (CLAW). That is, the feedback gains remain unchanged*. In the longitudinal axis, the stabilator is available as a redundant control effector on the UH-60 Black Hawk in moderate and high-speed cruise. A detailed explanation of the reconfiguration of the control mixer is presented in the following sections.

Control system design

The control system for the simulation model is designed based on model following linear dynamic inversion (DI). Model-following concepts are widely used in modern rotorcraft control systems for their ability to independently set feed-forward and feedback characteristics. The DI controller schedules the model with flight condition to eliminate the need for feedback gain scheduling due to similar error dynamics over different flight regimes. The controller is therefore applicable to a wide range of flight conditions (Refs. 17, 18). A schematic of the overall control system is shown in Figure 2. The control system mainly comprises of the inner and outer loop CLAWs. In the inner loop, the response type to pilot input is designed for Attitude Command Attitude Hold in the roll and pitch axis, where pilot input commands a change in roll and pitch attitudes ($\Delta\phi_{cmd}$ and $\Delta\theta_{cmd}$) and returns to the trim values when input is zero. The heave axis response type is designed for Rate Command Altitude Hold, where pilot input commands a change in rate-of-climb and holds current altitude when the rate-of-climb is zero. The yaw axis response type is designed for Rate Command Direction Hold, where pilot input commands a change in yaw rate and holds current heading when yaw rate is zero. The response type for the outer loop is Translational Rate Command, Position Hold, where pilot inputs command a change in ground speed and hold current inertial position when inputs are zero. With the implementation of the outer loop, the pilot input does not directly command $\Delta\phi_{cmd}$ *and* $\Delta\theta_{cmd}$ as in the inner loop CLAW. Rather, they are indirectly commanded through the desired ground speeds. For designing the CLAWS, the full 27-state linear model is reduced to an 8-state quasi-steady model whose state and control vectors are given by

$$\begin{aligned} \vec{x}_r &= [u, v, w, p, q, r, \phi, \theta]^T \\ \vec{u}_r &= [\delta_{lat}, \delta_{lon}, \delta_{col}, \delta_{ped}]^T \end{aligned} \quad (10)$$

Currently the main rotor RPM (Ω) is regulated via the throttle input determined by the RPM Governor as shown in Figure 2. Therefore, $\delta_{throttle}$ is truncated from the original control input vector. A more detailed explanation of the control system design is available in (Ref. 11).

Control Mixer

In the baseline simulation model, the control input vector $\vec{u}$ is comprised of two parts, namely $\vec{u}_{trim}$ and $\Delta\vec{u}$, where $\vec{u}_{trim}$ represents the reference trim input (determined by an off-line trim routine) to the aircraft and $\Delta\vec{u}$ denotes the change in control inputs from the feedback control laws (Fig. 2). The trim control inputs ($\vec{u}_{trim}$) are mapped to the main rotor swashplate servo actuators ($s_{lat}, s_{fwd}, s_{aft}$), and the tail rotor servo actuator (s_{ped}) through a control mixer, $\tilde{M}_{S/u}$ (Fig. 3) as shown in Eq. 11.

$$\begin{aligned} &\vec{S}_{trim} = \tilde{M}_{S/u}\vec{u}_{trim} \\ &where \quad \vec{S}_{trim} = [s_{lat}, s_{fwd}, s_{aft}, s_{ped}]^T_{trim} \end{aligned} \quad (11)$$

Similarly, $\Delta\vec{u}$ is mapped to the actuators through a control mixer ($\hat{M}_{S/u}$) as in Eq. 12.

$$\begin{aligned} &\Delta\vec{S} = \hat{M}_{S/u}\Delta\vec{u} \\ &where \;\; \Delta\vec{S} = [\Delta s_{lat}, \Delta s_{fwd}, \Delta s_{aft}, \Delta s_{ped}]^T \end{aligned} \quad (12)$$

The summation of the trim servo actuator inputs ($\vec{S}_{trim}$) and the change in servo actuator inputs ($\Delta\vec{S}$) from $\Delta\vec{u}$ are in turn mapped to the collective, lateral and longitudinal blade pitch

$(\theta_0, \theta_{1c}, \theta_{1s})$, and tail rotor collective pitch (θ_{tr}), through mechanical mixing $(M_{\theta/S})$ which is offset by a bias vector $(\vec{\theta}_{bias})$ as shown in Eq.13 (Ref. 12).

$$\vec{\theta} = M_{\theta/S}(\vec{S}_{trim} + \Delta\vec{S}) + \vec{\theta}_{bias} \tag{13}$$

The above equations are represented in the block diagram given in Fig. 3.

Baseline case (no failure): In the baseline case, Equation 14 represents the matrix form of the control mixer in both Eqs. 11 and 12. This shows the mapping between the control stick inputs and the individual actuator positions. These inputs are mixed such that change in a single control stick input results in a reduced off-axis response.

$$\tilde{M}_{S/u} = \hat{M}_{S/u} = \begin{bmatrix} m_{11} & 0 & m_{13} & 0 \\ 0 & m_{22} & m_{23} & m_{24} \\ 0 & m_{32} & m_{33} & m_{34} \\ 0 & 0 & m_{43} & m_{44} \end{bmatrix} \tag{14}$$

The baseline UH-60A simulation model has a moving stabilator, the position of which is given by a slew schedule (θ_{slew}) based on airspeed. The stabilator remains *inactive* as a feedback control effector in the baseline (no-failure) case.

Post-Failure: After an actuator failure (say *locked* s_{fwd}), the stabilator is brought in as a feedback control effector in the longitudinal axis. For the trim control inputs, $\vec{u}_{trim}$ (Eq. 11), the control mixer $(\tilde{M}_{S/u})$ is modified by setting the row corresponding to the failed actuator equal to zero in order to account for failure (Eq. 15). As for $\Delta\vec{u}$ (Eq. 12), an additional actuator (Δs_{stab}) that affects the stabilator is introduced in addition to the existing servo actuators; longitudinal stick input is then mapped to this control (Eq. 16). The element (m_{52}) in $\hat{M}_{S/u}$ is chosen such that 100% of longitudinal stick input corresponds to a full range of motion of the stabilator pitch. In this case, when s_{fwd} is *locked*, $\tilde{M}_{S/u} \neq \hat{M}_{S/u}$ (Eq. 15 and 16).

$$\tilde{M}_{S/u} = \begin{bmatrix} m_{11} & 0 & m_{13} & 0 \\ 0 & 0 & 0 & 0 \\ 0 & m_{32} & m_{33} & m_{34} \\ 0 & 0 & m_{43} & m_{44} \end{bmatrix} \tag{15}$$

$$\hat{M}_{S/u} = \begin{bmatrix} m_{11} & 0 & m_{13} & 0 \\ 0 & 0 & 0 & 0 \\ 0 & m_{32} & m_{33} & m_{34} \\ 0 & 0 & m_{43} & m_{44} \\ 0 & m_{52} & 0 & 0 \end{bmatrix} \tag{16}$$

Mechanical Mixer

The mechanical mixer $(M_{\theta/S})$ remains the same since it represents the mechanical rigging between the actuators and the blade pitches $(\vec{\theta})$ but now it also includes the mechanical rigging between the stabilator actuator (Δs_{stab}) and the change in stabilator incidence $(\Delta\theta_{stab})$. Equation 17 also includes an additional fail bias vector $(\vec{S}_{failbias})$ to account for the locked position of the failed actuator.

$$\vec{\theta} = M_{\theta/S}(\vec{S} + \Delta\vec{S} + \vec{S}_{failbias}) + \vec{\theta}_{bias} \tag{17}$$
$$where \quad \vec{S} = \left[s_{lat}, s_{fwd}, s_{aft}, s_{ped}, 0\right]^T,$$
$$\Delta\vec{S} = \left[\Delta s_{lat}, \Delta s_{fwd}, \Delta s_{aft}, \Delta s_{ped}, \Delta s_{stab}\right]^T,$$
$$\vec{S}_{failbias} = \left[0, s_{fail}, 0, 0, 0\right]^T$$

Equation 17 denotes the total input $\vec{\theta}$ to the plant model that is comprised of the trim $(\vec{\theta}_{trim})$ and control $(\Delta\vec{\theta})$ (Fig. 2). In the baseline (no-failure) case, the stabilator position is given by the slew schedule (θ_{slew}), which is appended to $\vec{\theta}$ (Eq. 18)

$$\vec{\theta} = \begin{bmatrix} \theta_{1c} \\ \theta_{1s} \\ \theta_{col} \\ \theta_{ped} \end{bmatrix} \longrightarrow \begin{bmatrix} \theta_{1c} \\ \theta_{1s} \\ \theta_{col} \\ \theta_{ped} \\ \hline \theta_{slew} \end{bmatrix} \tag{18}$$

Post-failure, the last entry in $\vec{\theta}$ (Eq. 19) contains the sum total of the stabilator slew schedule (θ_{slew}) and stabilator control input $(\Delta\theta_{stab})$, which is now mapped to the longitudinal stick.

$$\vec{\theta} = \begin{bmatrix} \theta_{1c} \\ \theta_{1s} \\ \theta_{col} \\ \theta_{ped} \end{bmatrix} \longrightarrow \begin{bmatrix} \theta_{1c} \\ \theta_{1s} \\ \theta_{col} \\ \theta_{ped} \\ \hline \theta_{stab} \end{bmatrix} \tag{19}$$
$$where \quad \theta_{stab} = \theta_{slew} + \Delta\theta_{stab}$$

The above equations are represented in the block diagram given in Fig. 4.

Control Coupling

In a dynamic inversion controller, the model of the aircraft dynamics is built into the controller through the state coupling and control coupling, CA and $(CB)^{-1}$ respectively. Here, A is the state evolution matrix, B is the control sensitivity matrix, and C is the output selection matrix. The control sensitivity matrix (B) calculated by the off-line trim routine relates the states and the main rotor collective and cyclic pitches, tail rotor collective, and stabilator pitch (represented by $\vec{\theta}$) whereas the controller commands changes in the pilot stick controls $(\vec{u}_r)$ (Fig. 14). Therefore, the control sensitivity matrix $(\hat{B})$ in the control coupling $((C\hat{B})^{-1})$ of the inner loop dynamic inversion of the controller can be represented by Eq. 20.

$$\hat{B} = BM_{\theta/S}\hat{M}_{S/u} \tag{20}$$

Post-failure, the partial reallocation of the longitudinal control to the stabilator through control mixer reconfiguration as described previously (Eq. 15 and 16) changes the control sensitivity $(\hat{B})$ through Eq. 20 which in turn brings change to the control coupling $((C\hat{B})^{-1})$ of the inner loop dynamic inversion of the controller.

RESULTS AND DISCUSSION

The following results are based on the simulation of a 16,000 lb UH-60A Black Hawk helicopter, as described in the modeling section. Figure 5 presents the trim sweep results for different forward actuator positions (in inches) for varying cruise speeds (in knots) with contours of stabilator angle of attack (in degrees). The feasible trim space is bounded by the maximum installed aircraft power, minimum blade flapping and the stabilator pitch hard stops as indicated on the figure. The colored portion of Fig. 5 shows that trim solutions exist for certain range of locked forward actuator positions at different cruise speeds when the stabilator is used as a redundant control. Trim solutions exist over a larger range of forward actuator positions at higher cruise speeds, shown by the increase in size of the colored section and attributed to the increased effectiveness of the stabilator at high speeds. In the present study, failure compensation and recovery of the aircraft are simulated and analyzed for a locked failure of the forward actuator position (s_{fwd}).

Forward Actuator Failure Compensation

The aircraft is simulated at a cruise speed of 120 knots represented by trim state A (Fig. 5). The forward actuator trim position for a cruise speed of 120 knots is 1.5 inches. Failure in the forward actuator (s_{fwd}) is modeled by raising the actuator 0.2 inches and locking it in position, represented by trim state B. Figure 6 presents the time history of the lateral, forward, and aft actuator positions (in inches) from 0 to 3 minutes at 120 knots. From 0 to 1.5 minutes, the trim positions of the three actuators at 120 knots are shown, at 1.5 minutes, the forward actuator (s_{fwd}) is moved by 0.2 inches and locked out of trim. As a result of which the aft actuator position (s_{aft}) decreases to a new trim position. Figure 7 shows the time history of the longitudinal cyclic pitch, θ_{1s} on the left axis and stabilator pitch incidence on the right axis. The increase in the forward actuator position along with reduction in aft actuator position results in the longitudinal cyclic pitch (θ_{1s}) becoming less negative (Fig. 7) which induces a nose-up pitching moment from the main rotor. At 1.5 minutes, the control mixer is reconfigured such that the stabilator is now part of the feedback system along the longitudinal axis (to account for the failed actuator). Hence, the stabilator pitches up from 3.2° (slew schedule shown by the dashed green line) to 8° (solid green line in Fig. 7) to produce a compensatory nose-down pitching moment.

The change in the longitudinal cyclic pitch (θ_{1s}) causes the rotor to flap back. This is clearly seen in Fig. 8, where the longitudinal flap (β_{1c}) decreases from 1.1° to −1°. This results a nose-up pitching moment and also decreases the propulsive force from the main rotor. In order to maintain the propulsive force, the vehicle orients to a more nose-down pitch attitude (−1.5° to −4°) (Fig, 9), enabled by the nose-down pitching moment produced by the stabilator.

The decrease in aft actuator position (s_{aft}) after locking s_{fwd} (Fig. 6) results in the collective pitch (θ_0) (Fig. 10) remaining unchanged.

Recovery

After successfully compensating for failure of the forward actuator through control mixer reconfiguration as shown in the previous section, aircraft recovery is now considered. The maximum forward touchdown speed is 60 knots ground speed (depicted by the vertical dashed red line in Fig. 11) on level terrain as described in the Operator's Manual for UH-60A helicopter (Ref. 19). The aircraft is commanded to slow down from the current trim state B (after failure compensation) at 120 knots to 50 knots, represented by trim state C (Fig. 11), after which the vehicle can be safely recovered by performing a rolling landing. Figure 12 shows the time history of the forward speed (in knots) from 2.5 to 10 minutes. At 3 minutes, the vehicle initiates the prescribed slow down from 120 to 50 knots that takes place over a period of 4 minutes. Figure 13 presents the time history for the lateral, forward, and aft actuator positions for the baseline and reconfigured aircraft. That is, the actuator positions the baseline aircraft would use to slow down are given by solid lines and the actuator positions the reconfigured aircraft after failure would use are represented by dashed lines. The locked position of forward actuator (s_{fwd}) considered for the simulation happens to be close to the trim position of the forward actuator of the baseline aircraft at 50 knots. Hence the remaining actuator positions also approach the baseline case (Fig. 13). Figure 14 shows the time history of the longitudinal cyclic pitch (θ_{1s}) for the reconfigured and baseline aircraft. The longitudinal cyclic pitch is more negative when compared to the baseline aircraft, resulting in a larger nose-down moment from the main rotor with respect to the baseline. The stabilator pitch in the reconfigured aircraft changes from 8° to 25°, this produces a smaller nose-down pitching moment compared to the baseline slew schedule (Fig. 15).

Figure 16 presents the longitudinal flap versus time for the reconfigured and baseline aircraft. The decrease in the longitudinal flap (β_{1c}) is smaller for the reconfigured aircraft, meaning the rotor flaps back less when compared to the baseline aircraft. Figure 17 presents the vehicle pitch attitude time history, where the initial nose-down pitch attitude becomes nose level in the reconfigured aircraft (indicated by the solid blue line). Change in the flapping and aircraft pitch attitude adjust to give the required propulsive force when compared to the baseline.

Post-forward actuator failure compensation and recovery simulation was successfully demonstrated for one case (trim state A → B → C). Note that a range of forward actuator positions exist (1.28 to 1.8 inches) where failure compensation and aircraft recovery can be attained within the safe landing speed limit (given by the horizontal dashed red lines in Fig. 11).

Aft Actuator Failure Compensation

Similarly, trim solutions exist for different aft actuator positions (s_{aft}) at varying cruise speeds and stabilator angle of

attack (Fig. 18). The feasible set of solutions is bounded by the stabilator pitch hard stops, minimum blade flapping and maximum installed power as was seen for the forward actuator. As the aft actuator position (s_{aft}) increases, longitudinal cyclic pitch (θ_{1s}) becomes more negative (Eq. 5) which results in the main rotor producing a nose-down pitching moment. In order to compensate, the stabilator angle of attack decreases, producing a nose-up pitching moment to achieve equilibrium. As such, as the locked position of the aft actuator increases (moving along the y-axis in Fig. 18), the corresponding trimmed stabilator angle of attack decreases. As with the forward actuator, a range of aft actuator positions exist (0 to 0.5 inches) where failure compensation and recovery of the aircraft within the safe landing speed limit is attainable (horizontal dashed red lines in Fig. 18). The stabilator hard stop prohibits motion beyond -8° which in turn reduces the amount of nose-up pitching moment that can be generated by the stabilator, therefore the trim solutions that do exist for aft actuator positions occur at lower values of actuator height than the forward actuator cases.

The range of locked actuator positions (s_{fwd} and s_{aft}) that allows for aircraft recovery to 60 kts correspond to a similar range of longitudinal cyclic pitch (θ_{1s}) for both the case of locked forward and aft actuator positions (Fig. 11 and 18). These values of θ_{1s} are a proxy for the pitching moment that is produced by the main rotor, which needs to be compensated by the stabilator. This range is approximately -5.8° to 0.3°, and is governed by the hard-stops on the stabilator pitch incidence, which limits the pitching moment that is achievable by the horizontal tail. The upper bound of the longitudinal cyclic in the case of locked aft actuator positions is not exactly the same as in the case of locked forward actuator position at 60 kts, due to the lower limit on the range of motion of the aft actuator.

Lateral Actuator Failure Compensation

It is possible to generate a roll moment from the horizontal tail by splitting it and applying a differential pitch. The ability of this differential stabilator to generate rolling moment could be used to compensate for a certain range of locked *lateral* actuator position in the same way that symmetric deflection of the stabilator has been shown to compensate for failure in the forward or aft actuators. Trim solutions exist for different lateral actuator positions (s_{lat}) at varying cruise speeds and differential stabilator pitch incidence (Fig. 19). Unlike the forward and aft actuators, only limits on the stabilator pitch hard stops and maximum installed power bound the feasible trim solutions. For a fixed lateral actuator position (s_{lat}) over some range of cruise speeds, there exists a differential stabilator pitch incidence ($\Delta\theta_{stab\ diff}$) which can compensate for failure, but recovery through rolling landing is limited with the differential stabilator because of the lack of feasible trim solutions for a wide range of lateral actuator positions (s_{lat}) at lower cruise speeds. That is, for any given cruise speed (say 120 kts), if the lateral actuator is locked in place, there are no feasible trim solutions at lower speeds (say 60 kts). This is primarily attributed to the insufficient roll moment arm for the stabilator.

CONCLUSIONS

The present study focuses on using the stabilator as a redundant control effector for main rotor swashplate servo actuator failure compensation in a UH-60A Black Hawk in cruise. A simulation model based on Sikorsky's GenHel model is modified to simulate and compensate for main rotor servo actuator failure. A model-following, linear dynamic inversion controller is implemented and modified to account for locked actuator positions. Upon failure of the forward (s_{fwd}) or aft actuator (s_{aft}), compensation is achieved by partial reallocation of longitudinal control to the stabilator through the control mixer because of its ability to generate pitching moments in forward flight. The mechanical mixer remains unchanged, only the control allocation between pilot stick input and aircraft actuator positions is modified. Longitudinal control is shared between the working actuator along the longitudinal axis (i.e. s_{aft}, if s_{fwd} is locked or vice versa) and the stabilator after failure. Control authority is assigned such that 100% of longitudinal stick corresponds to a full range of motion of the stabilator. The reallocation of authority to the stabilator changes the control coupling matrix, $(C\hat{B})^{-1}$, used in the feedforward path of the inner loop. However, the feedback control laws (feedback gains) remain unchanged. The following key conclusions can be drawn from this study:

- Steady-state trim solutions exist for a range of locked actuator positions at varying cruise speeds and stabilator angle of attacks. The stabilator pitch hard stops, minimum blade flapping and maximum installed power limits bound the feasible trim solutions.
- In the case of forward actuator failure (s_{fwd}), where its position is raised by 0.2 inches and locked out of trim, the longitudinal cyclic pitch (θ_{1s}) becomes less negative causing the rotor to flap back, which results in the main rotor producing a nose-up pitching moment. In the reconfigured aircraft, in order to compensate, the stabilator is moved to generate a nose-down pitching moment. Along with the change in flapping, the vehicle takes up a more nose-down pitch attitude so as to produce the required propulsive force. The aft actuator position (s_{aft}) decreases in order to hold the collective pitch (θ_0).
- The simulation demonstrates the reconfigured aircraft's capability to decelerate to less than 60 knots with the forward actuator locked in position. It is possible to recover the aircraft after failure compensation with a rolling landing within a certain range of locked forward actuator positions (1.28 - 1.8 inches).
- Similar to the forward actuator, trim solutions exist for different aft actuator positions (s_{aft}) at varying cruise speeds and stabilator angle of attacks. As with the forward actuator, a range of locked aft actuator positions

(0 - 0.5 inches) exist for which safe landing speed is attainable. Due to the stabilator pitch hard stop at -8°, the amount of nose-up pitching moment generated by the stabilator is limited. As a consequence of which trim solutions exist for the same range but at lower values of aft actuator locked positions relative to the forward actuator case.

- There exists a range of longitudinal cyclic pitch (θ_{1s}) (-5.8° to 0.3°) for aircraft recovery at 60 kts that corresponds to the recovery range of locked actuator positions observed in both the case of forward and aft actuator locked positions. This is a direct consequence of the stabilator pitch hard stops that govern the limits on the pitching moments produced by the stabilator in order to compensate for the main rotor pitching moments.
- It is possible for the horizontal stabilator to have lateral control authority and potentially compensate for swashplate lateral actuator (s_{lat}) failure by using a differential stabilator pitch ($\Delta\theta_{stab\ diff}$). Although failure compensation is possible over certain ranges of cruise speed, recovery with a rolling landing is possible for only a narrow range of locked lateral actuator positions. This is mainly due to relatively limited roll control authority the stabilator can provide.

Author contact:

Praneet Vayalali	vayalp@rpi.edu
Michael McKay	mckaym2@rpi.edu
Jayanth Krishnamurthi	krishj@rpi.edu
Farhan Gandhi	fgandhi@rpi.edu

REFERENCES

[1]Eslinger, Robert A and Chandler, Phillip R, "Self-repairing flight control system program overview," Aerospace and Electronics Conference,NAECON, Proceedings of the IEEE 1988 National, pp. 504–511, Dayton, OH, May 23–27, 1988.

[2]Stewart, James F and Shuck, Thomas L, "Flight-testing of the self-repairing flight control system using the F-15 highly integrated digital electronic control flight research facility," NASA-TM-101725, 1990.

[3]Bodson, Marc and Groszkiewicz, Joseph E, "Multivariable adaptive algorithms for reconfigurable flight control," IEEE transactions on control systems technology, 1997, Vol. 5, (2), pp. 217–229.

[4]Brinker, Joseph S. and Wise, Kevin A., "Flight Testing of Reconfigurable Control Law on the X-36 Tailless Aircraft," Journal of Guidance, Control, and Dynamics, 2001, Vol. 21, (5), pp. 903–909.

[5]Hess, Ronald A., "A Framework for Robust Rotorcraft Flight Control Design," Journal of the American Helicopter Society, April 2011, Vol. 56, (2), pp. 22004–22004.

[6]Heiges, Michael W., "Reconfigurable Controls for Rotorcraft A Feasibility Study," Journal of the American Helicopter Society, July 1997, Vol. 42, (3), pp. 254–263.

[7]Enns, Russell and Si, Jennie, "Helicopter Flight-Control Reconfiguration for Main Rotor Actuator Failures," Journal of Guidance, Control, and Dynamics, 2003, Vol. 26, (4), pp. 572–584.

[8]Reddinger, Jean-Paul and Gandhi, Farhan, "Using Redundant Effectors to Trim a Compound Helicopter with Damaged Main Rotor Controls," American Helicopter Society 73rd Annual Forum, Fortworth, TX, May 2017.

[9]Drozeski, G. R. and Saha, B. and Vachtsevanos, G. J., "A Fault Detection and Reconfigurable Control Architecture for Unmanned Aerial Vehicles," 2005 IEEE Aerospace Conference, pp. 1–9, MT, March 05–12, 2005.

[10]Qi, Xin and Theilliol, Didier and Qi, Juntong and Zhang, Youmin and Han, Jianda and Song, Dalei and Wang, Ling and Xia, Yong, "Fault diagnosis and fault tolerant control methods for manned and unmanned helicopters: a literature review," Control and Fault-Tolerant Systems (SysTol), 2013 Conference on, pp. 132–139, Nice, France, October 09–11, 2013.

[11]Krishnamurthi, Jayanth and Gandhi, Farhan, "Flight Simulation and Control of a Helicopter Undergoing Rotor Span Morphing," Journal of the American Helicopter Society, Vol. 63, No. 1, January 2018.

[12]Howlett, J.J., "UH-60A Black Hawk Engineering Simulation Program: Volume I - Mathematical Model," NASA CR-166309, 1981.

[13]Peters, D.A., and HaQuang, N., "Dynamic Inflow for Practical Applications," Journal of the American Helicopter Society, October 1988, Vol. 33, pp. 64–66.

[14]Bailey, F.J., "A Simplifed Theoretical Method of Determining the Characteristics of a Lifting Rotor in Forward Flight," NACA Report 716, 1941.

[15]Padfeld, G.D., "Helicopter Flight Dynamics: The Theory and Application of Flying Qualities and Simulation Modeling," Blackwell Publishing, 2nd ed., 2007.

[16]Ballin, M.G., "Validation of a Real-Time Engineering Simulation of the UH-60A Helicopter," Journal of the American Helicopter Society, NASA TM-88360, 1987.

[17]Stevens, B.L. and Lewis, F.L., "Aircraft Control and Simulation." John Wiley & Sons, 2nd ed., 2003.

[18]Tischler, M.B. and Remple, R.K.,"Aircraft and Rotorcraft System Identifcation: Engineering Methods with Flight Test Examples." AIAA, 2nd ed., 2012.

[19]Operators Manual for UH-60A, UH-60L, EH-60A helicopters, TM 1-1520-237-10, Headquarters, Department of the Army, Washington, D.C., 31 October, 1996.

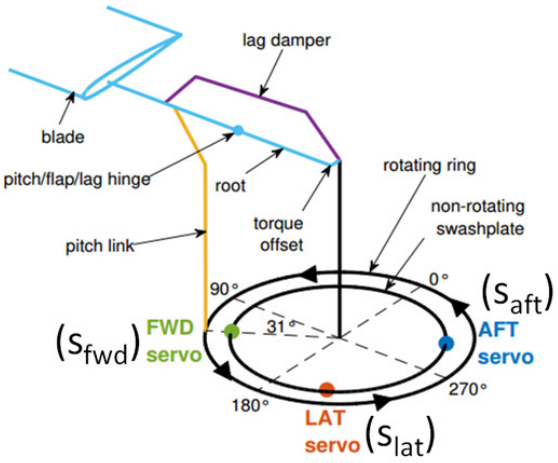

Fig. 1. Rotor Hub Model of a Single Blade at $\psi = 90°$ with Servo Locations Labeled

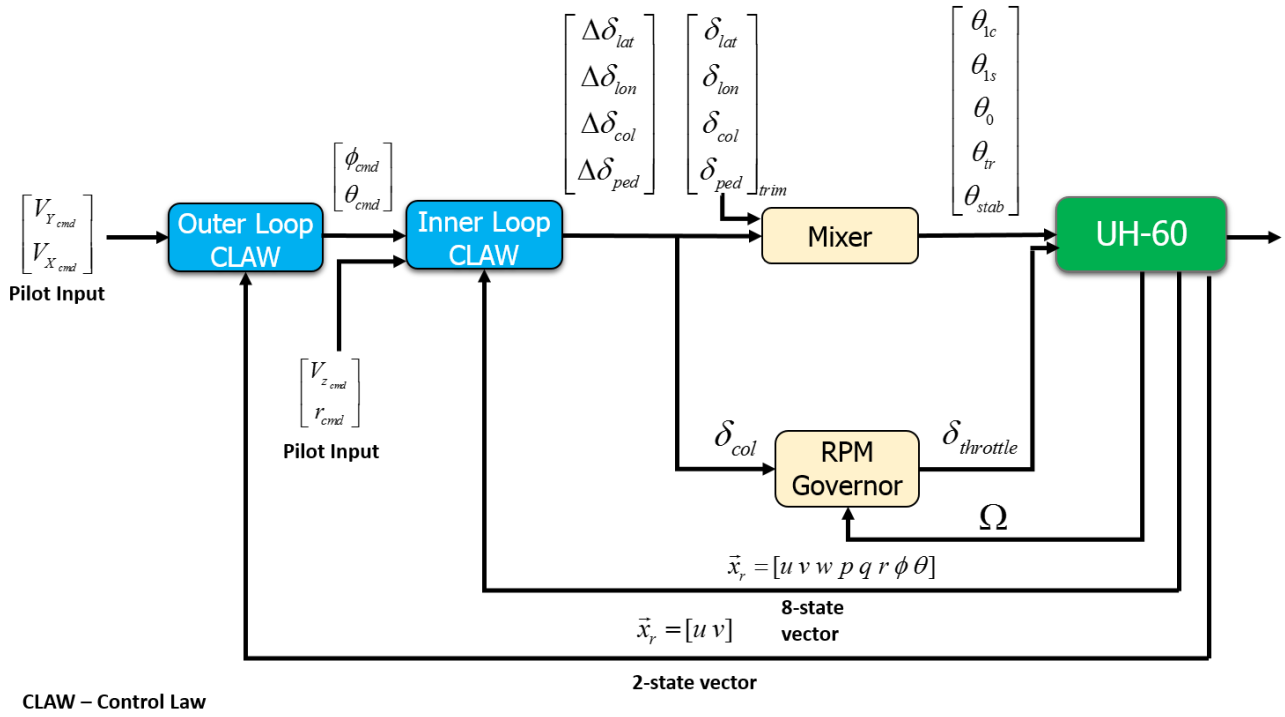

Fig. 2. Overview of the Control System

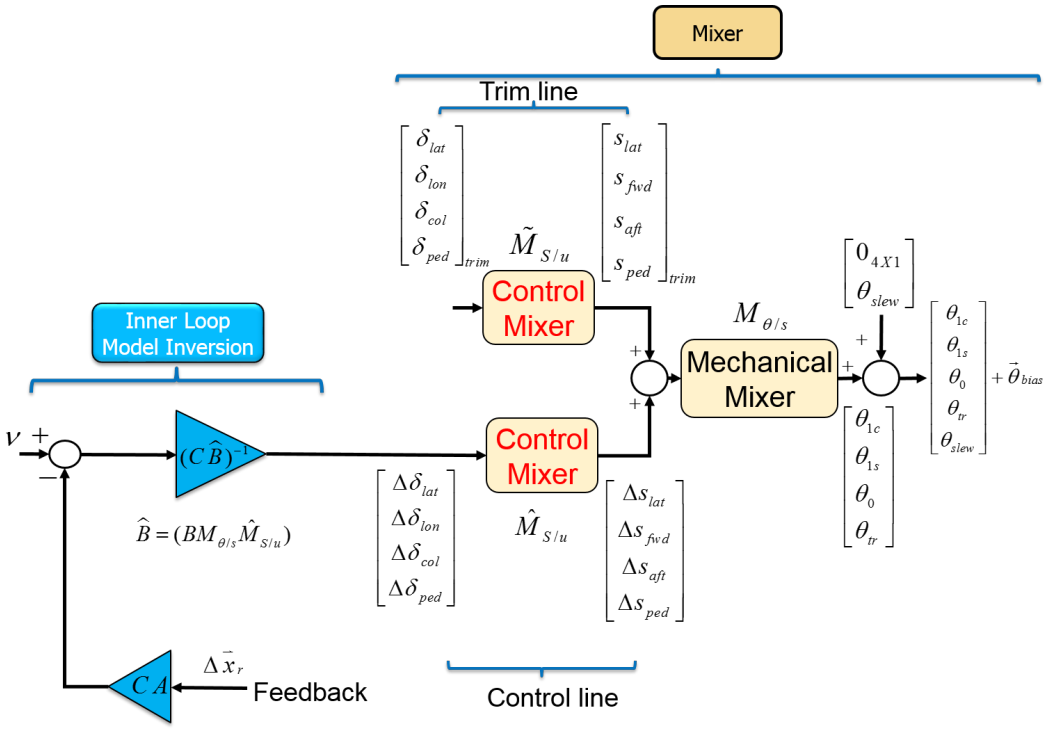

Fig. 3. Baseline Mixer

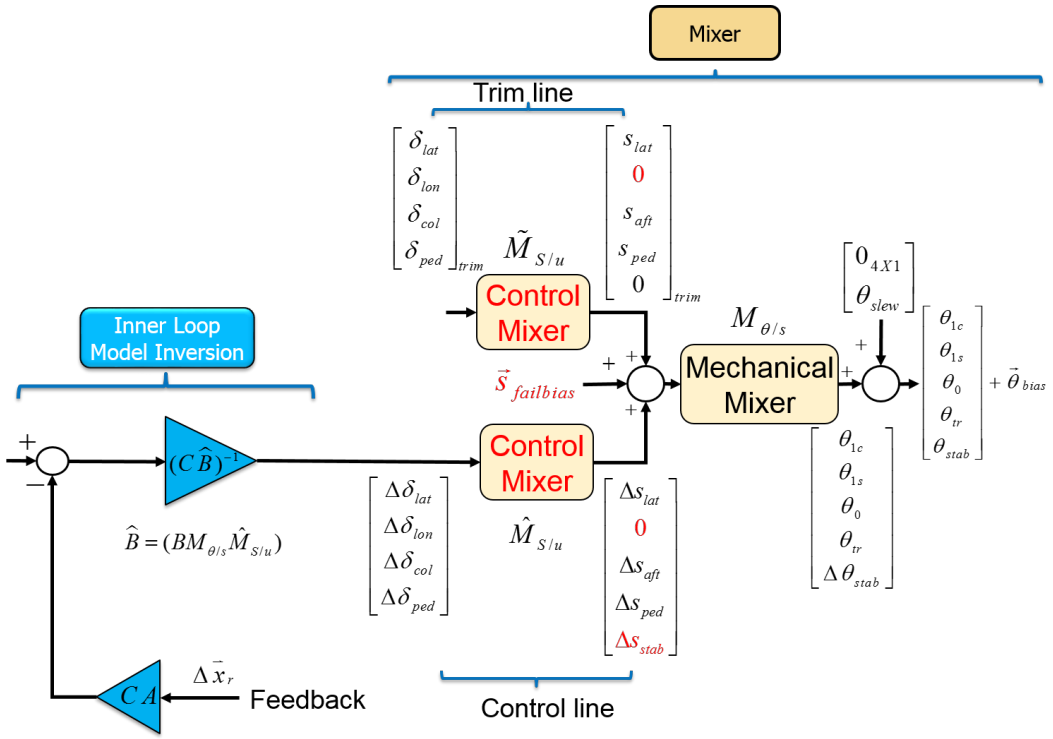

Fig. 4. Post-Failure Mixer

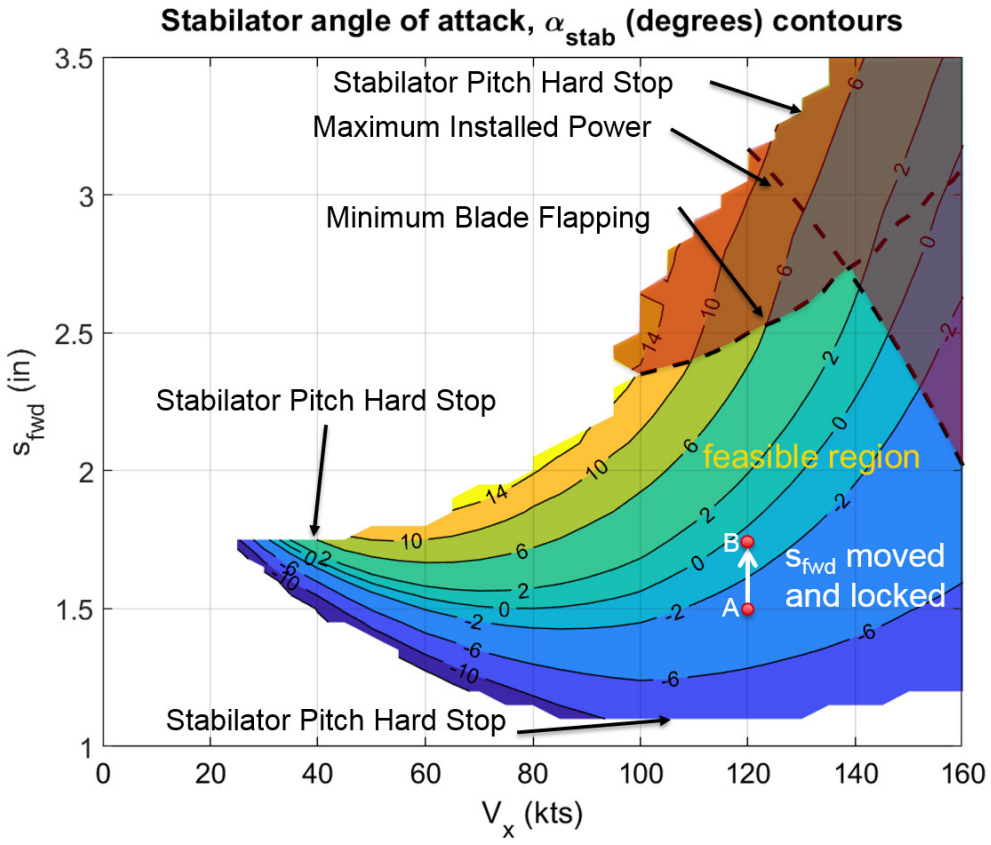

Fig. 5. Forward Actuator Velocity Trim Sweep

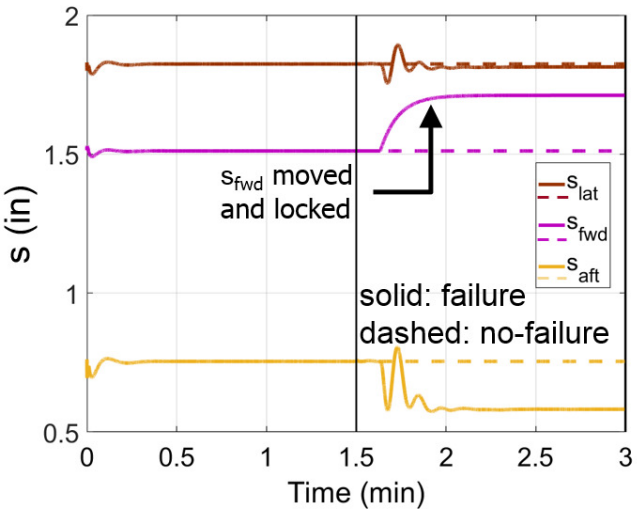

Fig. 6. Actuator Positions

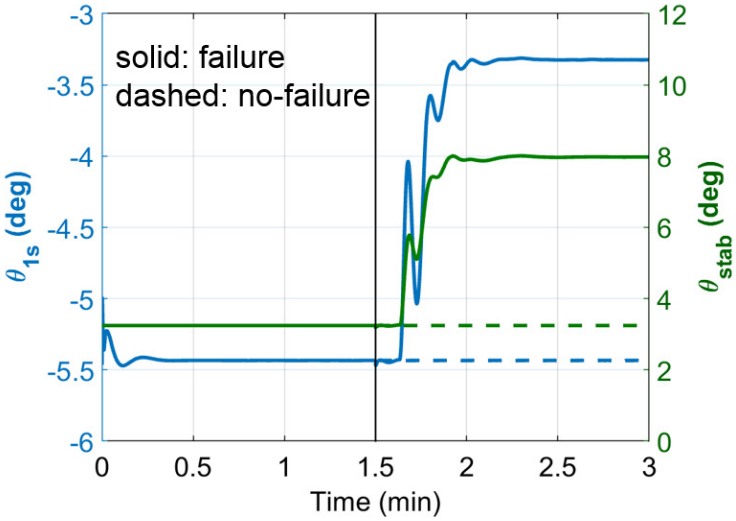

Fig. 7. Longitudinal Cyclic Pitch, θ_{1s}

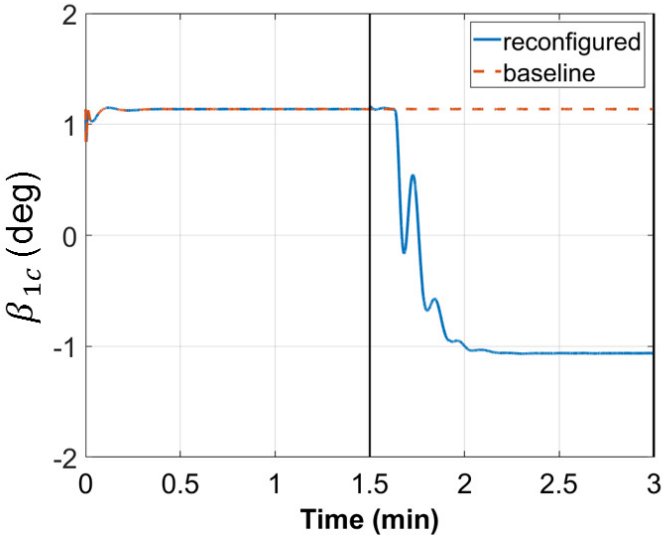

Fig. 8. Longitudinal Flap, β_{1c}

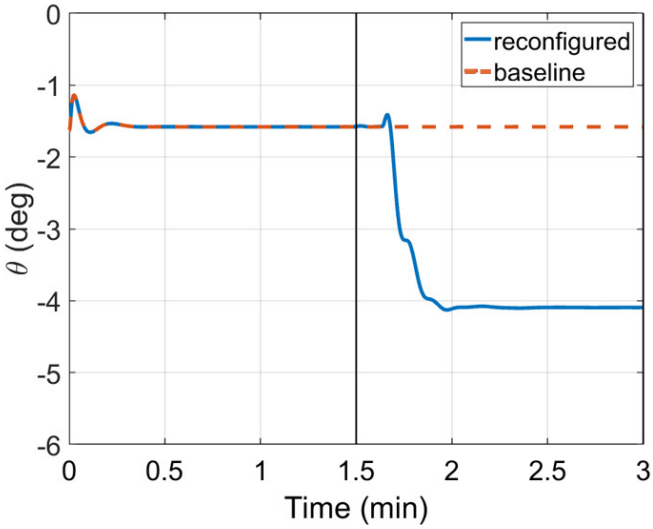

Fig. 9. Vehicle Pitch Attitude, θ

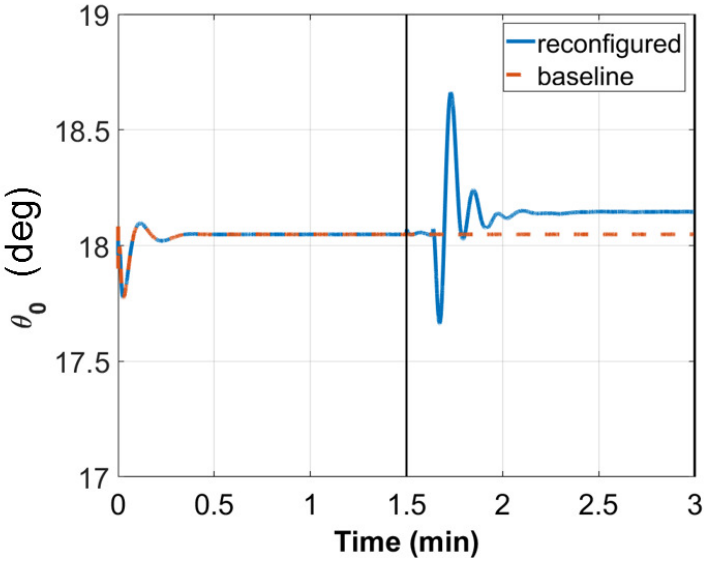

Fig. 10. Collective Pitch, θ_0

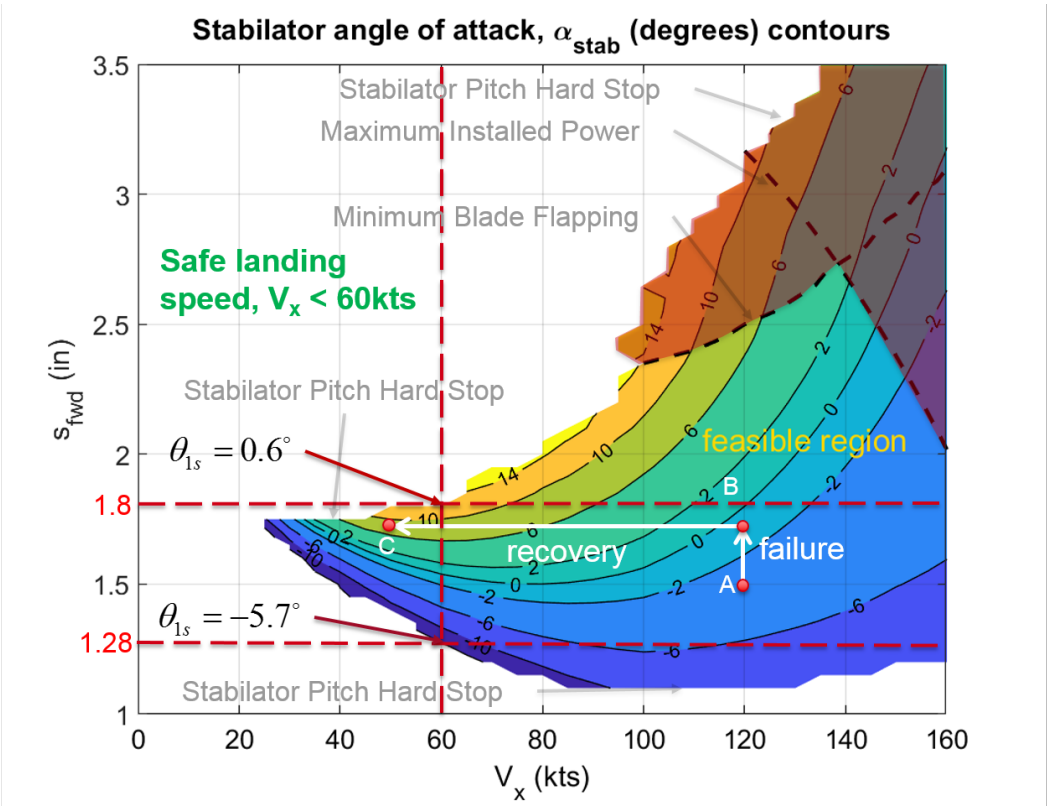

Fig. 11. Forward Actuator Velocity Trim Sweep

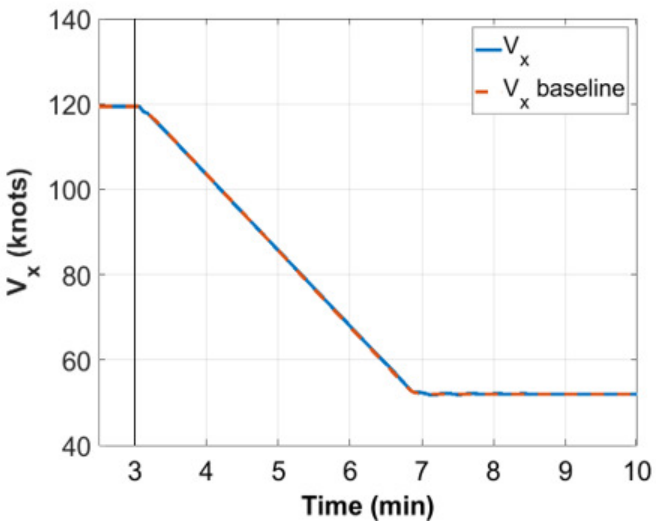

Fig. 12. Forward Speed, V_x

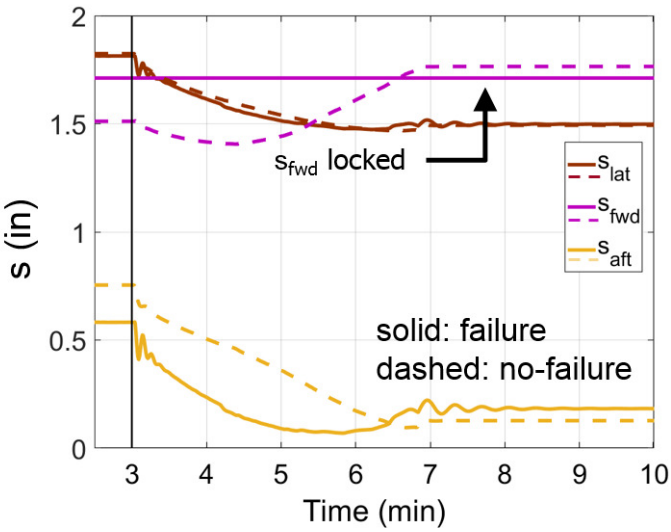

Fig. 13. Actuator Positions

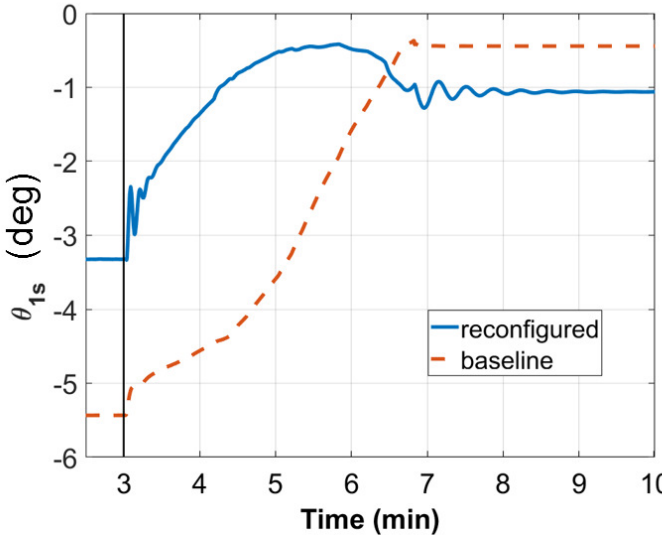

Fig. 14. Longitudinal Cyclic Pitch, θ_{1s}

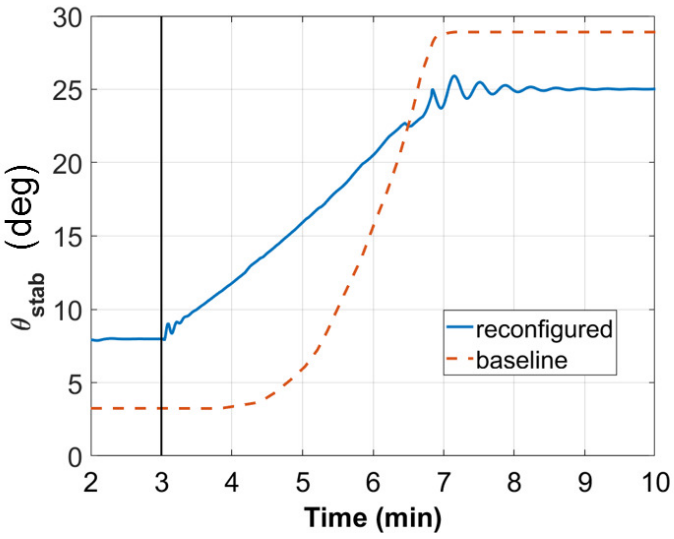

Fig. 15. Stabilator Pitch, θ_{stab}

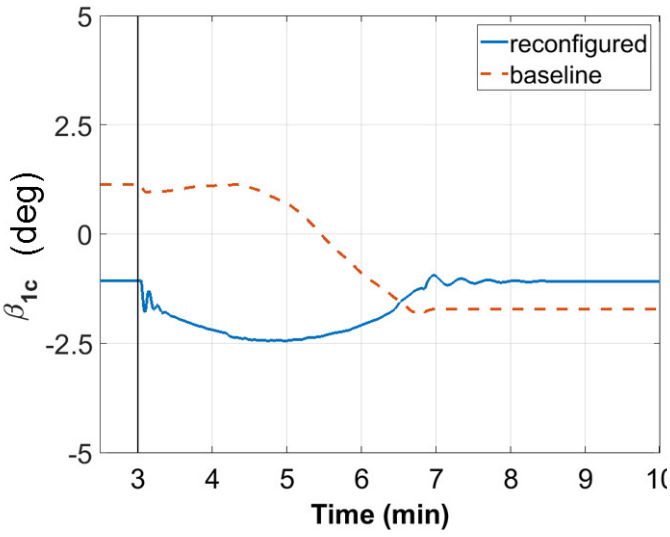

Fig. 16. Longitudinal Flap, β_{1c}

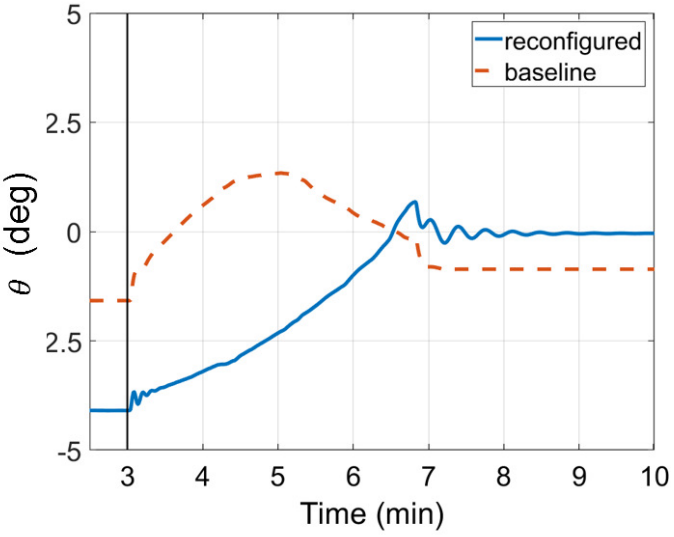

Fig. 17. Vehicle Pitch Attitude, θ

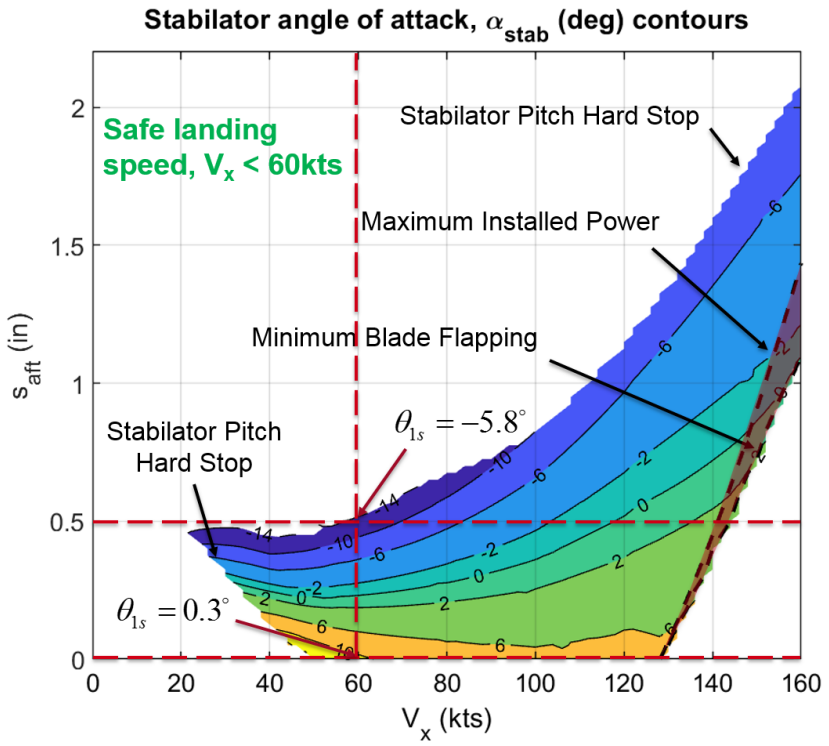

Fig. 18. Aft Actuator Velocity Trim Sweep

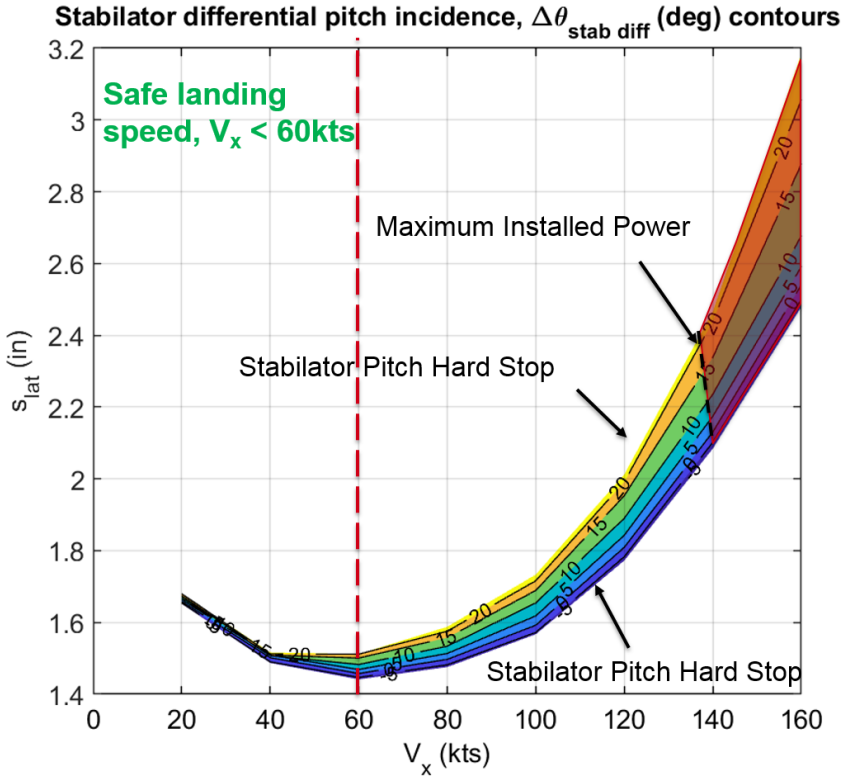

Fig. 19. Lateral Actuator Velocity Trim Sweep